HHS Public Access

Author manuscript

Int J Comput Assist Radiol Surg. Author manuscript; available in PMC 2019 June 17.

Published in final edited form as:

Int J Comput Assist Radiol Surg. 2018 June ; 13(6): 815–826. doi:10.1007/s11548-018-1744-4.

Ultrasound thermal monitoring with an external ultrasound source for customized bipolar RF ablation shapes

Younsu Kim[1], **Chloé Audigier**[1], **Jens Ziegle**[2], **Michael Friebe**[2], and **Emad M. Boctor**[1]

[1]Johns Hopkins University, 3400 N Charles Street, Baltimore, MD 21218, USA

[2]Otto-von-Guericke University, Universitaetsplatz 2, 39106 Magdeburg, Saxony-Anhalt, Germany

Abstract

Purpose—Thermotherapy is a clinical procedure which delivers thermal energy to a target, and it has been applied for various medical treatments. Temperature monitoring during thermotherapy is important to achieve precise and reproducible results. Medical ultrasound can be used for thermal monitoring and is an attractive medical imaging modality due to its advantages including non-ionizing radiation, cost-effectiveness and portability. We propose an ultrasound thermal monitoring method using a speed-of-sound tomographic approach coupled with a biophysical heat diffusion model.

Methods—We implement an ultrasound thermometry approach using an external ultrasound source. We reconstruct the speed-of-sound images using time-of-flight information from the external ultrasound source and convert the speed-of-sound information into temperature by using the a priori knowledge brought by a biophysical heat diffusion model.

Results—Customized treatment shapes can be created using switching channels of radio frequency bipolar needle electrodes. Simulations of various ablation lesion shapes in the temperature range of 21–59 °C are performed to study the feasibility of the proposed method. We also evaluated our method with ex vivo porcine liver experiments, in which we generated temperature images between 22 and 45 °C.

Conclusion—In this paper, we present a proof of concept showing the feasibility of our ultrasound thermal monitoring method. The proposed method could be applied to various thermotherapy procedures by only adding an ultrasound source.

Keywords

Thermal monitoring; Speed-of-sound reconstruction; Ultrasound; RFA modeling; Bipolar ablation; Hyperthermia; Ablation therapy; Thermotherapy

Correspondence to: Emad M. Boctor.

Compliance with ethical standards

Conflict of interest The authors declare that they have no conflict of interest.

Ethical approval For this type of study formal consent is not required.

Informed consent This article does not contain patient data.

Introduction

Thermotherapy is a clinical procedure delivering thermal energy for various medical applications including tumor ablation and drug delivery. Radio frequency ablation (RFA) has become a common procedure to treat malignant tissues using heat generated from alternating radio frequency electrical currents. Lately, bipolar RF ablation devices have been developed to treat tissues with user-defined shapes [1]. Thermotherapy requires heating the target tissues precisely and completely as well as preserving surrounding healthy tissues. Therefore, temperature monitoring is crucial for successful minimally invasive thermal procedures. Thermometers are often incorporated at the RF ablation probe tips, but they provide temperature information at only one or few measured points. Those local temperature measurements are not sufficient to monitor the overall thermal ablation procedure and assess a total coverage of the target volume. Instead, medical imaging techniques are needed to monitor the temperature in a 3D volume or at least in a 2D plane.

Ultrasound is a non-ionizing medical imaging modality and has the advantages of cost-effectiveness, high frame rate and portability. Attenuation and speed-of-sound (SOS) of ultrasound waves change with temperature. By using these properties, various ultrasound thermal or ablation monitoring methods have been proposed [2], including thermal strain method [3], Nakagami imaging [4] and quantitative ultrasound [5]. Those ultrasound thermal monitoring methods often detect indirectly the change in SOS and attenuation through quantitative measurements. For example, thermal strain imaging methods calculate the cross-correlation from echo shift caused by the SOS change and thermal expansion [3].

Ultrasound tomography is a technique which generates ultrasound attenuation or SOS images, directly reflecting the temperature change. Ultrasound tomography reconstruction techniques generally require a circular ultrasound gantry to transmit and receive the signals from multiple angles [6], but the required data acquisition time for the multiple projections degrades the temporal resolution. Robot-assisted ultrasound tomography where two conventional ultrasound probes are aligned has also been proposed [7]. This approach does not require a special ultrasound array design, but utilizes a robot control unit. In this paper, we propose an ultrasound thermal monitoring method which requires a minimal addition to a conventional RFA procedure: A single ultrasound source is integrated to the inserted ablation probe. The time-of-flight (TOF) information between this source and an ultrasound probe is acquired. The TOF changes during the ablation procedure can be detected in real time and used for temperature image reconstruction. Reconstructing SOS from limited-angle TOF information is an ill-posed optimization problem. Isotherm and regularization have been used to reconstruct SOS with limited-angle dataset in order to propose a ultrasound tomography thermometry [8]. Here, we use computational RFA modeling to provide the necessary a priori knowledge [9].

State-of-the-art MR thermometry has been used to evaluate the proposed SOS reconstruction method for the monitoring of high-intensity focused ultrasound [10]. In this work, we use the method to monitor the temperature generated by a customized RFA device. In this paper, we present a sensitivity analysis using in silico data. We also evaluate our ultrasound thermal monitoring method on two ex vivo experiments to show its feasibility.

Ultrasound thermal monitoring with an ultrasound source

Monitoring setup for a bipolar RF device

The proposed ultrasound thermal monitoring method utilizes a conventional ultrasound probe and an external ultrasound source. The region of interest (ROI) is the monitored ultrasound image plane. During RFA, the clinician introduces the ablation needles into the target area. The ultrasound element can be attached to one of the tines of the ablation probe; therefore, it could be inserted simultaneously within a monitoring plane as illustrated in Fig. 1.

The external ultrasound source can receive and transmit ultrasound pulses. In this paper, the ultrasound source transmits ultrasound pulses going through the ablation volume. TOFs are acquired by synchronizing the sampling and the pulser device.

Computational RFA modeling

We aim to recover the SOS in each pixel of the ROI; however, the maximal number of equations corresponds to the number of probe elements which is generally less than the number of pixels in ROI. A physics-based RFA simulation model is used to cope with the sparsity of the recorded TOF data. The number of unknowns is reduced by grouping pixels together with an equality constraint. In the same layer, pixels which are expected to have the similar temperature are grouped according to the RFA model.

$$\rho_t c_t \frac{\partial T}{\partial t} Q + \nabla \cdot \left(d_t \nabla T \right) + R\left(T_{b0} - T \right). \quad (1)$$

The Pennes model [11] is used, where ρ_t, c_t, d_t are the density, heat capacity, and conductivity of the tissue. T_{b0}, R, Q are blood temperature, reaction term, and source term modeling the heat brought by the RF ablation probe. The reaction term R becomes 0 as we are dealing with ex vivo tissue. In in vivo scenario, the reaction coefficient can be chosen to match target tissues [12,13]. This physics-based RFA simulation models the heat propagation in biological tissue using a reaction–diffusion equation, implemented using the lattice Boltzmann method (LBM) [9]. In the case of bipolar RFA, we assume the RF electrodes to be two independent sources and their temperatures are imposed as Dirichlet boundary conditions. Then, we are able to reconstruct thermal images with a limited number of equations by using prior knowledge provided by the physics-based RFA simulation model.

Acoustic speed-of-sound change during RF ablation

The temperature increases during a RFA procedure, and it consequently causes SOS changes in the ablation zone. The TOFs collected from each probe element change accordingly. The relation between the SOS and the temperature can be expressed with polynomial fit models [14]. The SOS is measured between 17.5 and 54.5 °C for a 2% agar and 2% silicon dioxide phantom which has similar properties of tissues [10]. In this paper, we use a SOS against temperature curve defined by Eq. 2, where T is the temperature in °C and SOS is the speed-of-sound in m/s.

$$\begin{aligned} \mathrm{SOS} = & -1.32\times10^{-5}T^4 + 2.134 \\ & \times10^{-3}T^3 - 1.569\times10^{-1}T^2 \\ & +7.451T + 1395.744 + \mathrm{SOS}_{\mathrm{offset}}. \end{aligned} \quad (2)$$

We assume that for all ex vivo tissue, their SOS against the temperature curves have similar trends, and we add a variable $\mathrm{SOS}_{\mathrm{offset}}$ in the equation to account for different tissues. The $\mathrm{SOS}_{\mathrm{offset}}$ is evaluated before ablation by using $\mathrm{SOS}_{\mathrm{init}}$ and T_{init}, the initial temperature. $\mathrm{SOS}_{\mathrm{init}}$ is the SOS of the tissue before the ablation starts. It is estimated from the acquired TOF before ablation simultaneously to the estimation of the US element location. The element localization is described in detail in "Computational RFA modeling" section. The T_{init} can be the body temperature or measurements from a thermometer if available.

Ultrasound element localization

The element localization with respect to the ultrasound probe is performed before an ablation procedure. First, the B-mode image can be used to assess the coarse positioning in the image plane. However, the preset SOS parameter in the ultrasound imaging system does not necessarily correspond to the actual SOS of the target tissue, which could cause an error in the localization. Moreover, the ultrasound element can appear with side lobes in the B-mode image, which brings a segmentation error in the lateral axis. For these reasons, we estimate more precisely the ultrasound element location as follows:

$$\underset{p_{\mathrm{e}},\,\mathrm{SOS}_{\mathrm{init}}}{\text{minimize}} \sum_{i=1}^{N} \left(\left\| p_{\mathrm{e}} - p_{\mathrm{p}i} \right\| - \mathrm{SOS}_{\mathrm{init}} \cdot \mathrm{TOF}_i \right)^2, \quad (3)$$

where p_{e} is a 2D vector that contains axial and lateral position of the element in the ultrasound image plane and $p_{\mathrm{p}i}$ is the ith probe element location. N denotes the number of elements in the ultrasound imaging probe. TOF_i is the ultrasound signal TOF between the ith probe element and the external ultrasound element. We consider $\mathrm{SOS}_{\mathrm{init}}$ as an unknown and estimate it since each target tissue would have different SOS. Thus, the total number of unknowns is three including initial SOS, axial and lateral location of the element. The estimated $\mathrm{SOS}_{\mathrm{init}}$ is used to calculate $\mathrm{SOS}_{\mathrm{offset}}$ in Eq. 2. This localization can be performed again when the monitoring system detects patient motion from sudden TOF changes.

Speed-of-sound reconstruction

The ultrasound pulses propagate through the ablation volume, so the TOFs change along with the SOS change around the ablation region during the procedure. In the image plane, we have K number of pixels, which corresponds to a product of number of image pixels in axial and lateral axis. The 2D image becomes a K length vector, and the pixel number k is defined as the kth element in this vector. We estimate the SOS in each pixel k of the image plane. This SOS_k contributes to the TOF_i with the intersection length l_{ik}, where i is the ultrasound element number in the ultrasound imaging probe. The l_{ik} is illustrated in Fig. 2a.

It is the intersection length of the propagation path u_i at a pixel k. The intersection length can be calculated for each pixel [15]. This l_{ik} is nonzero if the pixel k lies on the straight propagation path u_i. The delta function has a value of 1 on the propagation path and 0 everywhere else. We define the effective monitoring area as a triangular region surrounded by the edge propagation paths u_1 and u_N.

$$\mathrm{TOF}_i = \sum_{k=1}^{K} \delta(u_i) l_{ik} / \mathrm{SOS}_k . \quad (4)$$

l_{ik} is computed with the localized coordinate of the external ultrasound source. They compose a system matrix L, which has a size of N by K. The vector x in Eq. 5 is the inverse of SOS in the pixel. We eventually solve a least square problem presented in Eq. 5.

$$\begin{aligned} &\underset{x}{\text{minimize}} \ \left\| Lx - \mathrm{TOF} \right\|^2 \\ &\text{subject to} \ \ \bar{\mathrm{SOS}}_0 = \mathrm{SOS}_{\text{init}} \\ &1/\mathrm{SOS}_{\max} \le x \le 1/\mathrm{SOS}_{\min} \\ &\bar{\mathrm{SOS}}_j \le \bar{\mathrm{SOS}}_{j-1}, \ \ \text{for } j > 1 \end{aligned} \quad (5)$$

$$T_{\text{step}} = \max\left(T_{\mathrm{C}}, (T_{\max} - T_{\min})/\mathrm{Layer}_{\max}\right). \quad (6)$$

The matrix L is typically a wide matrix since the number of pixels K is greater than the number of equation N. To solve the ill-posed optimization problem, we apply equality conditions to reduce the unknown number. An equality condition is created based on the RFA bio-heat model. An example is shown in Fig. 2b. The simulated temperature image is divided into multiple labels using a temperature step, T_{step}, to obtain a label image. As described in Eq. 6, T_{step} is determined based on the maximum temperature difference divided by a chosen maximum label number, $\mathrm{Layer}_{\max}$, or based on a constant temperature T_{C}. Our system chooses the larger one of the two numbers. T_{C} and $\mathrm{Layer}_{\max}$ are user-defined constants. Each pixel is labeled based on the simulation results, and we consider the pixels whose label is the same have equal SOS. The pixels whose SOS is not expected to change are considered as background pixels. Those background pixels are labeled as 0, and the equality condition of initial SOS and $\bar{\mathrm{SOS}}_0$ holds for them. $\bar{\mathrm{SOS}}$ is SOS in each labeled pixel. The pixels with the same jth label have the same SOS value $\bar{\mathrm{SOS}}_j$ in Eq. 5. $\mathrm{SOS}_{\min}$ is background SOS which can be equivalent to initial SOS. $\mathrm{SOS}_{\max}$ is the possible maximum SOS in the temperature range between initial temperature and 100 °C from Eq. 2.

SOS against temperature curve calibration

SOS images can be recovered using the acquired TOF. To convert them to temperature images, a SOS against temperature curve is necessary. Those curves vary among tissues, but

if they are known, the conversion could be performed for each tissue in inhomogeneous structures. This SOS against temperature curve can be calibrated using various methods. For example, it can be obtained by measuring the TOF at different temperatures using an ultrasound pitch–catch geometry with the known distance between ultrasound sensors. This approach assumes that the entire tissue between the sensors has homogeneous temperature, which can be challenging at high temperatures. We propose another calibration method for our thermal monitoring method, based on TOF data and thermometer tip readings. As state-of-the-art ablation devices have one or several thermometers at their ablation tips, we assume that we know the temperature at the ablation center. We reconstruct SOS images during an ablation procedure, and then we fit a polynomial equation with the temperature readings and the reconstructed SOS at the ablation center.

Experiments and results

Sensitivity analysis using in silico experiments

Speed-of-sound reconstruction—We generated ground truth temperature images using the bio-heat model simulation. A bipolar ablation protocol consisting of 8 min of heating followed by 2 min of cooling was simulated to mimic a clinical scenario. Model parameters used previously for the validation of RFA simulation using porcine liver tissues were used [12]. We considered two different patterns. A horizontal pattern is created by activating two electrodes at the tip, and a diagonal pattern ablation is achieved by activating the crossing electrodes. Temperature images in two different imaging planes were converted into SOS images using the conversion Eq. 2. We define the pixel coordinate as (lateral, axial in mm scale) in the ultrasound image. The 128 ultrasound probe elements are located between (0.79, 0) and (59.21, 0) with a pitch size of 0.46 mm. The ground truth temperature ranged between 21 and 59 °C including the room temperature and the ablation temperature (Fig. 3).

The ultrasound element was located at (25.5, 55.5), and we set the heating center at (30.5, 27.5). TOF sets were acquired based on the SOS images and geometric location of the ultrasound probe and an external ultrasound element. TOF vector has a size of N, which is 128 in this experiment (Fig. 4).

To mimic a soft tissue [16] ablation, SOS_{init} was set at 1500 m/s and T_{init} at 21°. Those values can be arbitrarily chosen since SOS_{offset} in Eq. 2 is estimated to calibrate the SOS against temperature curve.

In this case, $TSOS_{offset}$ is estimated at −0.243 m/s. We set the maximum label numbers to 40, and the constant temperature step between the layer to 0.5 °C. With these parameters, the number of equation is always approximately 3 times larger than the number of labels, so the least square optimization can be solved in a stable manner.

Over the ablation, 67.2 and 90.1 % of the images had a maximum error of less than 1 and 2 °C. However, the error becomes larger when the maximum temperature exceeds 50 °C. In the conversion curve between SOS and temperature, the first-order derivative becomes smaller as the temperature increases to 60 °C. For this reason, when we convert the SOS to the temperature, it could result in larger temperature errors with small SOS differences. The

maximum errors in the images over the 600s for the four patterns were 0.43 ± 0.22, 1.39 ± 0.90, 0.42 ± 0.23 and 1.47 ± 1.11 °C.

Ultrasound element location—The ablation is centered at (30.5, 27.5) as shown in Fig. 5. It was converted from temperature image which has a maximum variation of 14 °C. The corresponding SOS image has a maximum difference of 36 m/s. Simulations were performed at 180 different ultrasound element locations, which include the depth of 40, 50 and 60 mm at lateral location from 0.5 to 59.5 mm with 1-mm intervals. To avoid an error in the intersection length calculation algorithm [15], a small number of 10^{-9} mm is added to the element location in the lateral axis. The system matrix L in Eq. 5 was computed. It took 0.0234±0.0026s for 60 by 60 pixel images over 180 trials.

At the depth of 50 and 60 mm, the reconstruction accuracy is fairly stable along the whole lateral axis. However, the reconstructed image shows errors when the element is located on the side in shallow depths. This is because the effective monitoring region does not cover the entire ablation volume. Some propagation paths do not go through the ablation region, but only background pixels; thus, the SOS in some layers cannot be calculated accurately. These TOFs do not contribute to solving the SOS in heated area. On the other hand, when the ultrasound element is located around the central axis, the error increases even though the effective monitoring region covers widely the ablation volume. At this location, the TOF change is almost symmetric, dividing by two the number of useful information. This explains the large error when the element is placed in the middle position.

SOS against temperature curve calibration and sensitivity analysis—Datasets from two different patterns, horizontal and diagonal, (second and forth setups in Fig. 3) are used for calibration since they present an ablation tip in the image plane. They both cover a temperature range between 21 and 59 °C. We define the ground truth curve generated from Eq. 2 as CGT. TOFs were generated using CGT, and then SOS images were reconstructed by solving Eq. 5. We fit a fourth-degree polynomial curve using the temperatures and the reconstructed SOS at the heating center. C1 and C2 are the generated calibration curves from the horizontal and diagonal pattern datasets, respectively. We compared C1 and C2 with CGT every 0.01 °C in the simulated temperature range. The mean square errors were 0.0587 and 0.0958 m/s for C1 and C2, respectively (Fig. 6).

We also analyzed the effect when a different curve was used to convert the SOS to the temperature. Two additional curves from the literature are used: the third-degree polynomial fit R1 [14] and the fifth-degree polynomial fit R2 [17] since the major component of the biological tissue is water. We calculated and applied SOS_{offset} to these curves to match SOS_{init} and T_{init}. The SOS_{offest} values were found to be −34.98 and 14.56 m/s for R1 and R2, respectively. The mean square errors of two curves compared to CGT were 4.28 and 1.63 m/s for the temperatures at every 0.01 °C in the range between 21 and 59 °C (Fig. 7).

Table 1 shows the maximum absolute error and the mean error averaged in all the pixels excluding the background pixels in each of the 600 images for the two patterns when we use different curves. The averaged maximum error over the 600 images increased by 0.10 and

0.13 °C compared to the results using CGT with C1 and C2 for the horizontal pattern. With R1 and R2, the averaged maximum error increased by 2.27 and 0.47 °C.

Ex vivo porcine liver experiment

We performed two ex vivo experiments with porcine livers as the setup shown in Fig. 1, but the ultrasound element was inserted through a hole from the liver surface. We used a bipolar ablation device to create two different patterns and provided power with a RF generator (Radionics Inc., USA). The channel data were captured with a linear L14-5W/60 (Ultrasonix Corp., Canada) ultrasound transducer and a SonixDAQ (Ultrasonix Corp., Canada) at 40 MHz sampling rate. The linear ultrasound probe has a 5–14 MHz bandwidth and a 10 MHz center frequency. An external function generator triggered the data collection and the ultrasound element pulse transmission every second. The ultrasound element was placed in the image plane using B-mode images, and we further adjusted its position using ultrasound channel data signal strength. The liver tissues were placed at room temperature during 12h for homogeneous temperature distribution. The tissues were ablated for 8 min and cooled for 1 additional minute. The ablation probes remained in the tissue during the cooling phase without providing RF power. Reference temperature was measured around 5 mm away (in lateral axis) from one of the bipolar needle tips and recorded every 30s.

Ultrasound element fabrication—We fabricated an external ultrasound source with a tube-shaped lead zirconate titanate (PZT) material. The element can transmit and receive ultrasound signals from its surface. The ultrasound element is connected to a coaxial cable, so it can be directly integrated with sampling or pulser devices. The tube-shaped PZT has an inner diameter of 2.2 mm and an outer diameter of 2.5 mm. The inner and outer surfaces are soldered with the core and the ground electrode in a coaxial cable. An epoxy material is filled in the tube for electrical insulating and acoustic backing.

Figure 8c illustrates the captured ultrasound signal propagating through a porcine tissue before and after an ablation procedure. A sample corresponds to 25-ns duration, and the shift due to the SOS change in the tissue is observed. The transmitted ultrasound signal was received by the linear L14-5W/60 ultrasound transducer. The center frequency of the received signal was 3.7 MHz, and its bandwidth was 2.5–5.6 MHz.

Temperature image reconstruction—Figure 9b, e illustrates the TOF change of four elements over the ablation procedures. We collected channel data every second for 9 min, so a total number of 540 ultrasound channel data were collected for each ablation lesion shape. For the first acquired channel data before the ablation starts, TOFs are estimated by finding the first peak which exceeds a threshold. This threshold was set to 6 times the standard deviation of signals from each element. For the following channel data, the TOF shifts are calculated using cross-correlation. Then, outliers are removed if the absolute TOF shift is larger than a threshold value. This threshold value of shifting samples was 25 samples (625 ns). These threshold values can be adjusted depending on the signal strength, ablation size and temperature.

The bipolar ablation probes were inserted in parallel, 2 cm apart from each other and fixed by a rigid holder. The ultrasound probe was placed in the middle plane between the ablation

probes as shown in Fig. 1, and the ultrasound channel data were collected with SonixDAQ. We set the maximum label numbers to 40, and the constant temperature step was 0.2 °C.

In the first experiment, the tissue temperature started at 22 °C and a horizontal ablation pattern was performed. After 1 min of the ablation, we detected an element motion of around 1 mm; thus, we re-localized the ultrasound element. The element location was identified at (39.03, 43.56), and the SOS_{init} was 1549.68 m/s. The corresponding SOS_{offset} in Eq. 2 was 46.29 m/s. The 114th element had the highest TOF change among the 128 probe elements for the horizontal lesion ablation.

The element in the second experiment was localized at (46.56, 54.19), and the SOS_{init} was 1549.66 m/s with an initial temperature of 23 °C. The SOSoffset was estimated as 43.24 m/s. The diagonal ablation pattern was tested. The 120th element showed the highest TOF change during the ablation. It started to decrease 2 or 3 samples after 1 min of ablation, while the TOFs of the ultrasound element numbers below 90 had rarely changed during the time. The maximum shift of TOF was 475 ns, which may propagate through the highest temperature region in the image plane. The overall temperature in the image increased as the ablation time elapsed.

Discussion and conclusion

Ultrasound thermal monitoring methods often suffer from patient motions and the uncertainty of random speckles. Even though the proposed method can also be affected by patient motion, the reconstruction algorithm can keep operating as long as the relative location of the ultrasound receiver and transmitting sources do not change. In addition, it is also possible to re-localize the ultrasound source and run the thermal monitoring algorithm again with prior SOS information. This has been applied in the first ex vivo experiment, and the monitoring algorithm had been restarted from the re-localized point after 1 min has elapsed. The result shows that the system can cope rapidly with the motion. In the proposed method, the ultrasound signals suffer less from attenuation compared to ultrasound echo signals since the waves only travel one way and received signals do not rely on reflection. Moreover, the ultrasound signal is actively generated from an external element, so the uncertainty caused by random speckles does not hinder the proposed approach.

Several aspects of the proposed approach can affect the SOS estimation accuracy. The ultrasound source position is adjusted by manually maximizing the strength of the pulse signal received by the ultrasound imaging probe. The effect would be minimized by using a mid-plane detection system [18].Moreover, the system can be improved with photoacoustic technique to generate omni-directional pulses with a minimal acoustic source size.

The biophysical modeling simulation also has an effect on the reconstruction results. First, the error changes depending on the temperature step constant and the number of labels used to generate the label segmentation image. Second, the sensitivity of the bio-heat simulation model to the tissue parameters employed can affect the accuracy of the proposed approach. The sensitivity of the parameters has been studied [12].

The SOS against temperature curve can be a critical factor. In this paper, we use a conversion curve measured from a tissue mimicking agar phantom and introduce an offset to compensate for SOS in different tissues by using the initial temperature and SOS. We also presented a method to calibrate this curve by using the acquired TOF and temperature measured by a thermometer during the ablation. To cope with various tissue types, we could estimate different SOS to temperature curves. Nonetheless, even with the use of different curves, we showed reasonable accuracy of the reconstructed thermal images. The proposed method was validated with heterogeneous ex vivo tissues, assuming homogeneous tissue properties. However, it can be further improved to cope with inhomogeneous tissues, frequently treated in the practical scenarios. Indeed, the RFA biophysical model supports the temperature estimation for complex structures. For instance, it has been used to simulate RFA close to blood vessels [9]. Information from prior or intra-operative medical image can be used as inputs, and heterogeneous tissue structures can be taken into account in order to reconstruct SOS images more accurately.

In clinical scenarios, the proposed ultrasound thermal monitoring system can be performed with conventional ultrasound imaging systems. Since the proposed method does not require high frame rate, B-mode images and channel data can be acquired alternately and the thermal images could be overlaid on the B-mode images. The system enabling these features could be developed on currently available ultrasound systems to translate the proposed method for clinical application in the future. The ultrasound element could be integrated to a RFA probe by attaching it to one of the ablation tines or by adding an extra wire. Therefore, it would not increase the invasiveness nature of the common radio frequency ablation procedures performed nowadays.

In this paper, we presented a proof of concept of an ultrasound thermal monitoring method. Simulation and ex vivo porcine liver experiments of various customized ablation lesion shapes using a novel bipolar RFA system were performed. The proposed method is not limited to the thermal monitoring of RFA for tumor tissues. For example, it can also be combined with radiation therapy and used to monitor hyperthermia for drug delivery.

In vivo experiments will be performed in the future to validate the robustness of our methods to patient motion, and more validations using multiple thermometers or a thermochromic phantom could be performed to study the custom RFA device behavior [19].

Acknowledgments

The research reported in this paper was supported by the National Institute of Biomedical Imaging and Bioengineering of the National Institutes of Health under Award Number R01EB021396 and National Science Foundation under Proposal Number 1653322.

References

1. Ali, G; Krug, JW; Friebe, M. A four-electrode radiofrequency ablation system designed for more complex and tumor specific ablation patterns. Proceedings of BioSpine 2017, 6th international Congress on biotechnologies for spinal surgery; 2017.
2. Lewis MA, Staruch RM, Chopra R. 2015; Thermometry and ablation monitoring with ultrasound. Int J Hyperth. 31(2):163–181.

3. Seo CH, Shi Y, Huang S-W, Kim K, O'Donnell M. 2011; Thermal strain imaging: a review. Interface Focus. 1(4):649–664. [PubMed: 22866235]
4. Zhang S, Zhou F, Wan M, Wei M, Quanyou F, Wang X, Wang S. 2012; Feasibility of using Nakagami distribution in evaluating the formation of ultrasound-induced thermal lesions. J Acoust Soc Am. 131(6):4836–4844. [PubMed: 22712954]
5. Ghoshal G, Luchies AC, Blue JP, Oelze ML. 2011; Temperature dependent ultrasonic characterization of biological media. J Acoust Soc Am. 130(4):2203–2211. [PubMed: 21973375]
6. Duric N, Boyd N, Littrup P, Sak M, Myc L, Li C, West E, Minkin S, Martin L, Yaffe M, Schmidt S, Faiz M, Shen J, Melnichouk O, Li Q, Albrecht T. 2013; Breast density measurements with ultrasound tomography: a comparison with film and digital mammography. Med Phys. 40(1): 013501. [PubMed: 23298122]
7. Aalamifar F, Khurana R, Cheng A, Guo X, Iordachita I, Boctor EM. 2017; Enabling technologies for robot assisted ultrasound tomography. Int J Med Robot Comput Assist Surg. 13(1):e1746.
8. Norton SJ, Testardi LR, Wadley HNG. Oct.1983 Reconstructing internal temperature distributions from ultrasonic time-of-flight tomography and dimensional resonance measurements. 1983 ultrasonics symposium. :850–855.
9. Audigier C, Mansi T, Delingette H, Rapaka S, Mihalef V, Carnegie D, Boctor E, Choti M, Kamen A, Ayache N, Comaniciu D. 2015; Efficient lattice boltzmann solver for patient-specific radiofrequency ablation of hepatic tumors. IEEE Trans Med Imaging. 34(7):1576–1589. [PubMed: 30132760]
10. Kim Y, Audigier C, Ellens N, Boctor EM. 2017A novel 3D ultrasound thermometry method for HIFU ablation using an ultrasound element. 2017 IEEE international ultrasonics symposium (IUS). :1–4.
11. Pennes HH. 1998; Analysis of tissue and arterial blood temperatures in the resting human forearm. J Appl Physiol. 85(1):5–34. [PubMed: 9714612]
12. Audigier C, Mansi T, Delingette H, Rapaka S, Passerini T, Mihalef V, Jolly M-P, Pop R, Diana M, Soler L, Kamen A, Comaniciu D, Ayache N. 2017; Comprehensive preclinical evaluation of a multi-physics model of liver tumor radiofrequency ablation. Int J Comput Assist Radiol Surg. 12(9):1543–1559. [PubMed: 28097603]
13. Payne S, Flanagan R, Pollari M, Alhonnoro T, Bost C, O'Neill D, Peng T, Stiegler P. 2011; Image-based multi-scale modelling and validation of radio-frequency ablation in liver tumours. Philos Trans R Soc Lond A Math Phys Eng Sci. 369(1954):4233–4254.
14. Sun Z, Ying H. 1999; A multi-gate time-of-flight technique for estimation of temperature distribution in heated tissue: theory and computer simulation. Ultrasonics. 37(2):107–122. [PubMed: 10209554]
15. Siddon RL. 1985; Fast calculation of the exact radiological path for a three-dimensional CT array. Med Phys. 12(2):252–255. [PubMed: 4000088]
16. Rice DA. 1983; Sound speed in pulmonary parenchyma. J Appl Physiol. 54(1):304–308. [PubMed: 6826415]
17. Belogol'skii VA, Sekoyan SS, Samorukova LM, Stefanov SR, Levtsov VI. 1999; Pressure dependence of the sound velocity in distilled water. Meas Tech. 42(4):406–413.
18. Guo X, Kang H-J, Etienne-Cummings R, Boctor EM. 2014; Active ultrasound pattern injection system (AUSPIS) for interventional tool guidance. PLoS ONE. 9(10):1–13.
19. Mikhail AS, Negussie AH, Graham C, Mathew M, Wood BJ, Partanen A. 2016; Evaluation of a tissue-mimicking thermochromic phantom for radiofrequency ablation. Med Phys. 43(7):4304–4311. [PubMed: 27370145]

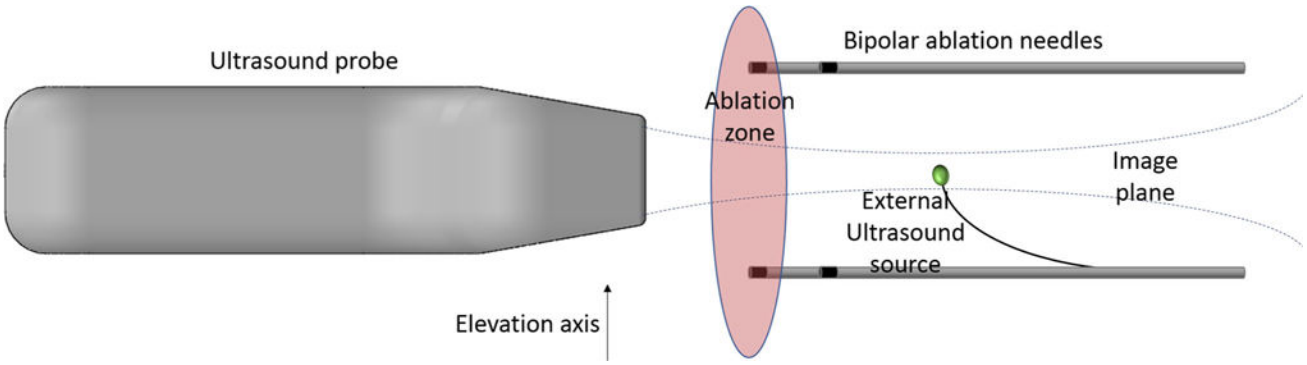

Fig. 1.
Proposed ultrasound thermal monitoring setup for RFA with bipolar needles

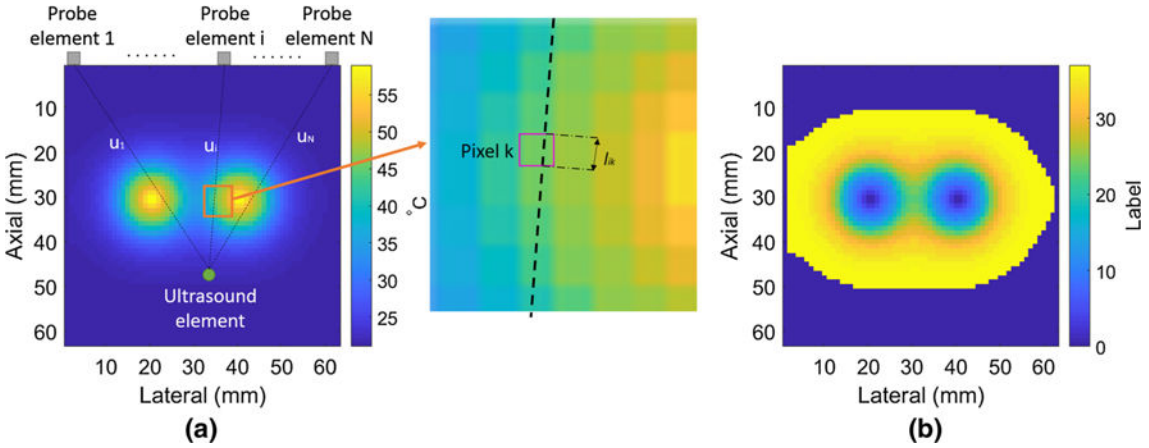

Fig. 2.

a A temperature image generated by the bio-heat simulation with a bipolar needle setup. The external element and the imaging plane elements are shown. The geometrical relationship used in the text are also detailed. **b** The corresponding label segmentation image generated with T_{step} = 0.5 °C and $Layer_{max}$ = 40

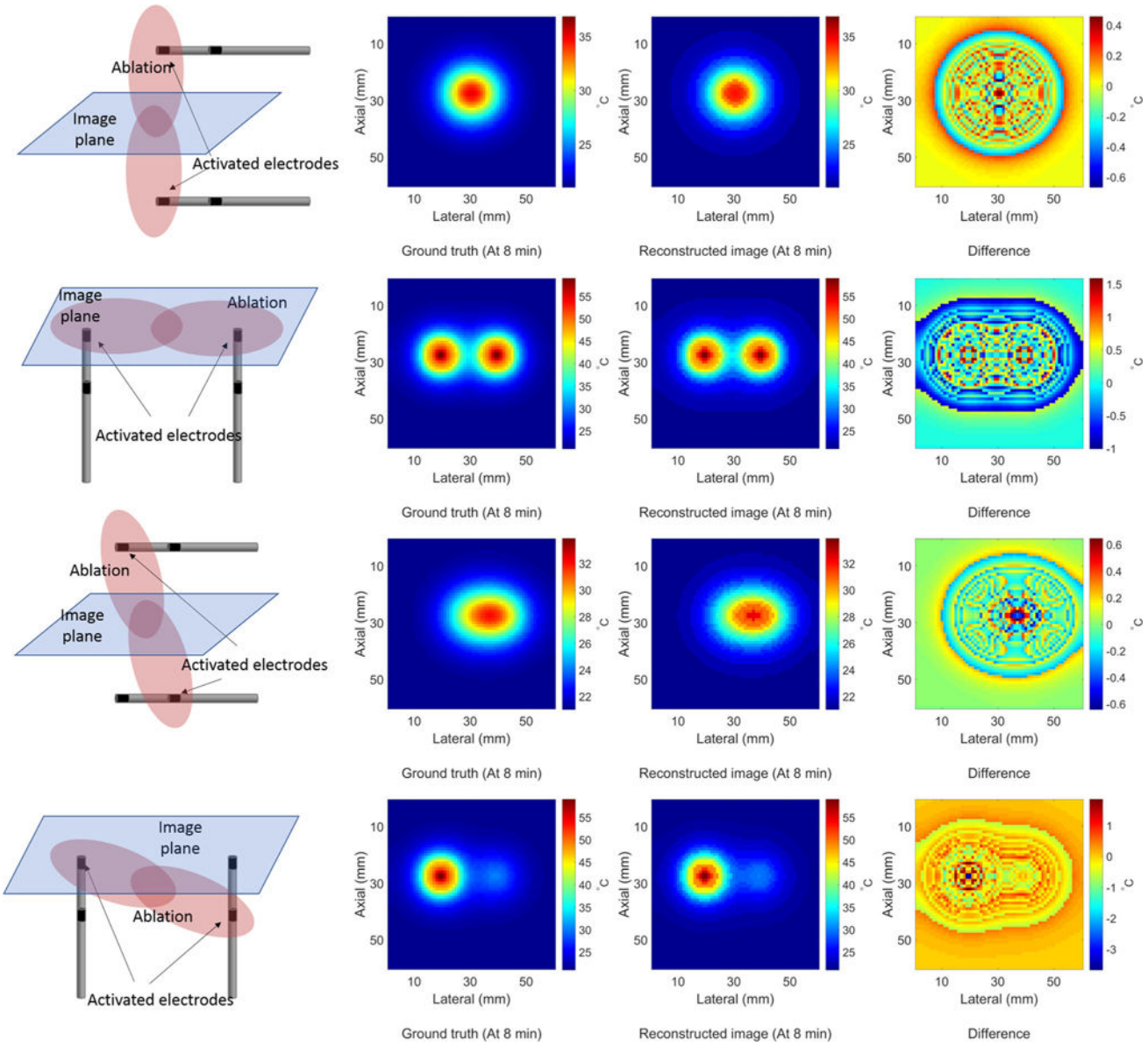

Fig. 3.

The simulation setup, a simulated temperature image, their corresponding reconstructed temperature images and the difference between them (at 8 min after ablation)

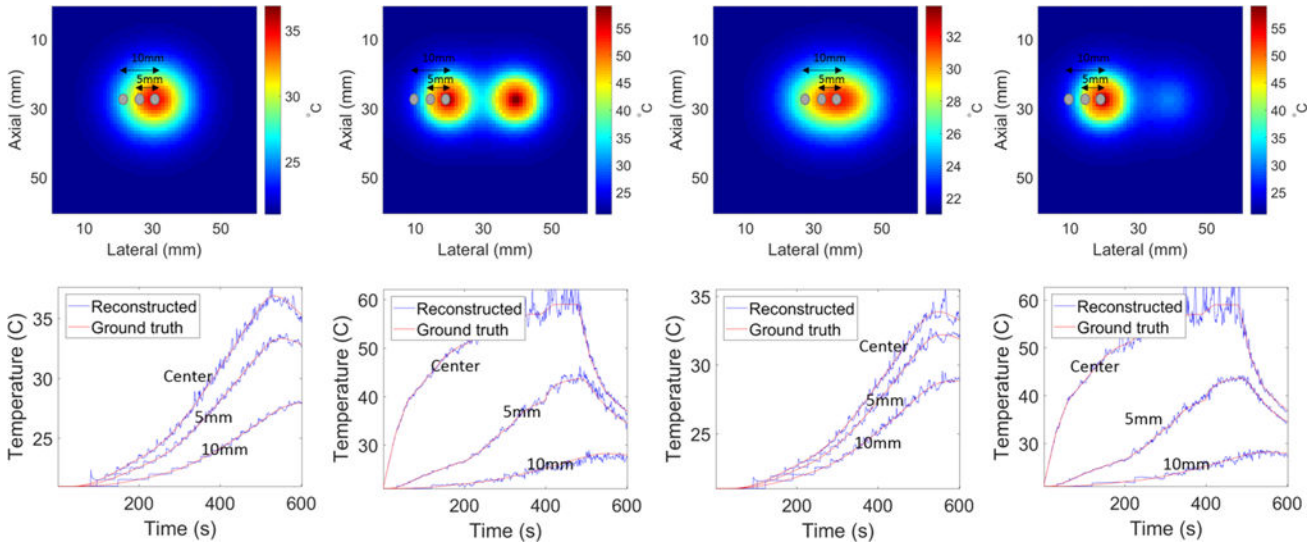

Fig. 4.

Upper images show four temperature images for each setup depicted in Fig. 3. Three evaluated temperature points are also visible: at the ablation center, and 5 and 10 mm away from the center in lateral axis. The graphs at the bottom show those temperature changes over time

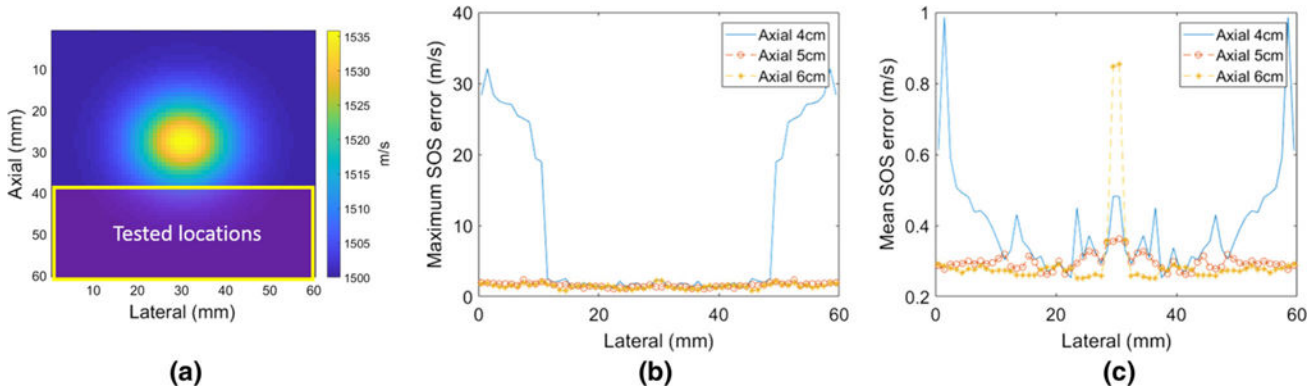

Fig. 5.

Ultrasound element location study: **a** simulated SOS image and tested locations. **b** Maximum error. **c** Mean error

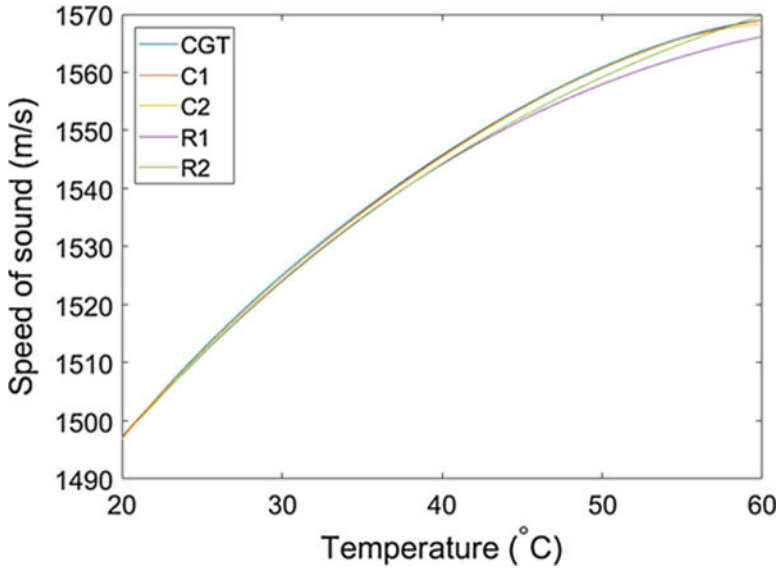

Fig. 6.

The calibrated curves C1 and C2, and the reference curves R1 and R2 are compared to the ground truth curve CGT

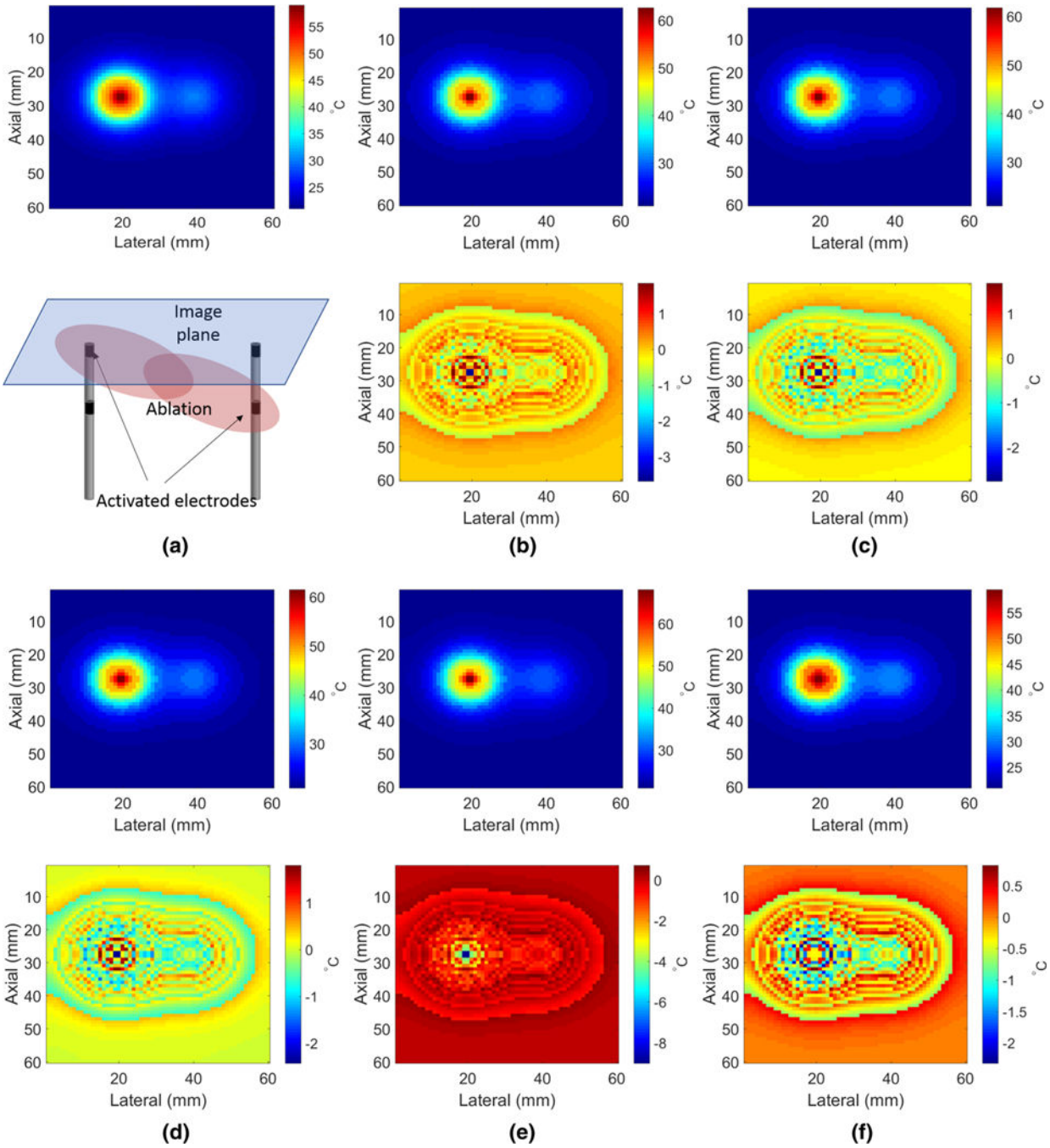

Fig. 7.

Examples of reconstructed temperature images and errors using different converting curves for the diagonal pattern (at 8 min). **a** The ground truth temperature image and the setup geometry. **b** CGT. **c** C1. **d** C2. **e** R1. **f** R2

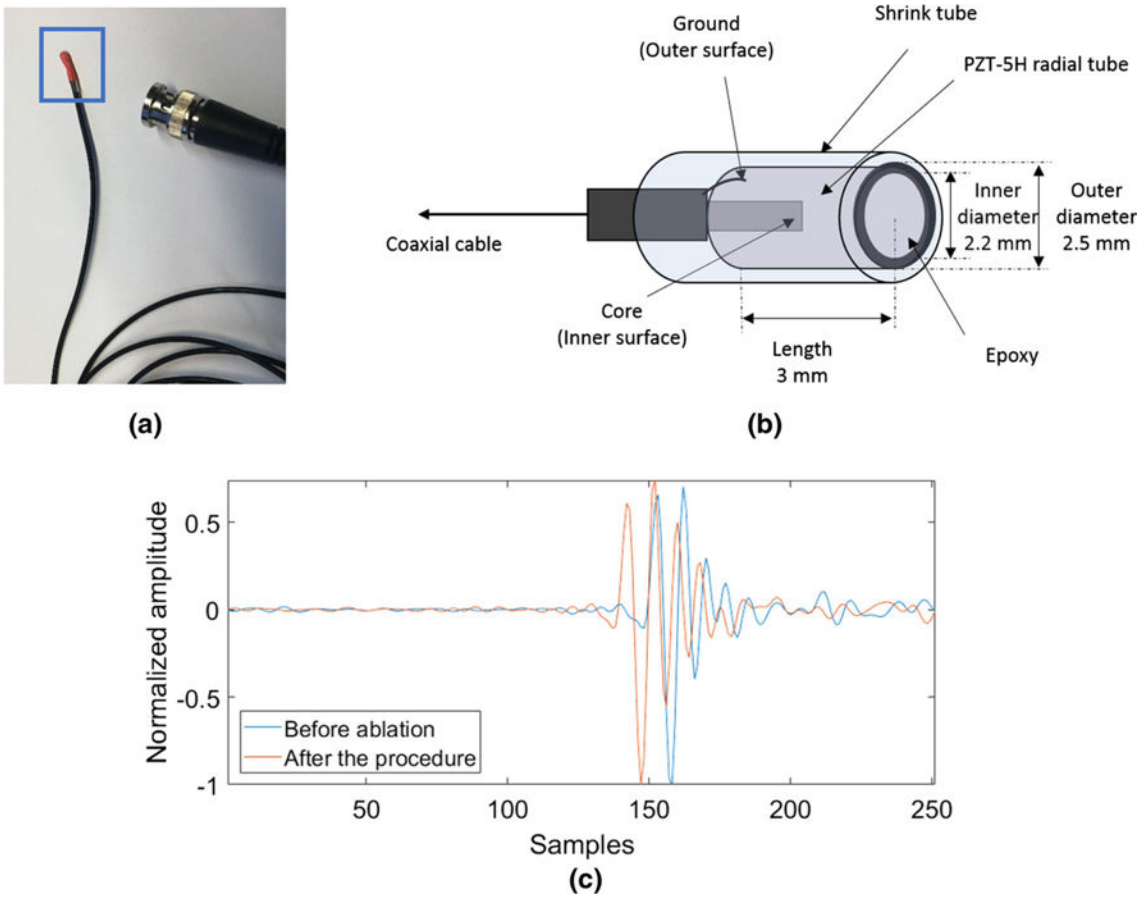

Fig. 8.

a Fabricated ultrasound element. **b** The ultrasound element structure. **c** Captured ultrasound signal transmitted by the ultrasound element through a liver tissue

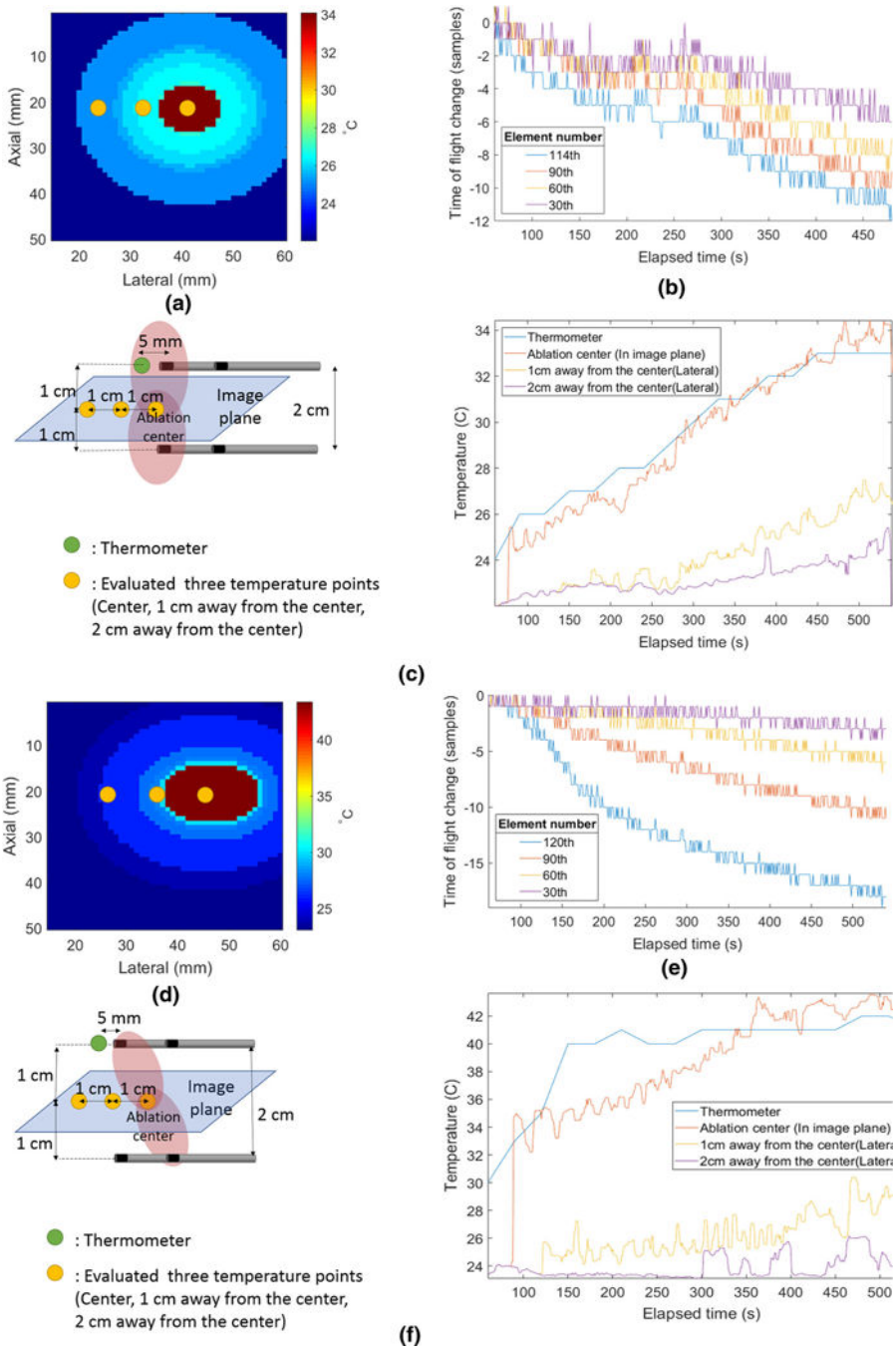

Fig. 9.

Experiment results for horizontal and diagonal patterns. **a**, **d** The reconstructed thermal image at $t = 8$ min. **b**, **e** TOF change over time at 4 different probe elements. **c**, **f** The estimated temperature at three different points in the image plane compared with a thermocouple measurement at 5 mm away from the tip in the lateral direction. The jitter was filtered using the seventh-order median filter, and the noise levels (standard deviation) of the

three points were 0.7418, 0.4055 and 0.3664 °C for the horizontal pattern, while the noise levels of the three points were 3.4318, 1.6621 and 1.1788 °C for the diagonal pattern

Table 1

Errors using different SOS against temperature curves averaged over 600 frames

Pattern\curve	CGT	C1	C2	R1	R2
Maximum errors (°C)					
Horizontal	1.39 ± 0.90	1.49 ± 0.92	1.52 ± 1.08	3.66 ± 2.55	1.86 ± 0.86
Diagonal	1.47 ± 1.11	1.49 ± 1.01	1.48 ± 1.07	3.60 ± 2.70	1.82 ± 0.85
Mean errors (°C)					
Horizontal	0.35 ± 0.20	0.38 ± 0.19	0.36 ± 0.20	0.52 ± 0.26	0.46 ± 0.21
Diagonal	0.27 ± 0.12	0.30 ± 0.11	0.28 ± 0.12	0.38 ± 0.14	0.36 ± 0.11